International Journal of Minerals, Metallurgy and Materials
Volume 26, Number 1, January 2019, Page 86
https://doi.org/10.1007/s12613-019-1712-1

Azole derivatives embedded in montmorillonite clay nanocarriers as corrosion inhibitors of mild steel

Milad Edraki and Davood Zaarei

Polymer Department, Technical Faculty, South Tehran Branch, Islamic Azad University, Tehran, P.O. Box 11365-4435, Iran
(Received: 3 March 2018; revised: 8 May 2018; accepted: 10 May 2018)

Abstract: Azole derivatives such as 2-mercaptobenzothiazole (MBT) and 2-mercaptobenzimidazole (MBI) were introduced as corrosion inhibitors into the interlayer space of sodium montmorillonite clay (Na^+-MMT). The corrosion protection behavior of mild steel in solutions containing MBT, MBI, MMT + MBT, MMT + MBI, Na^+-MMT, and NaCl (3.5wt%) was evaluated using polarization and electrochemical impedance spectroscopy (EIS). Also, the release of penetrated species into the medium from the clay nanocarriers was evaluated using ultraviolet-visible (UV-Vis) spectroscopy. Small-angle X-ray scattering (SAXS) confirmed the insertion of MBT and MBI into the inner space of the clay layers and the interaction between two organic and inorganic phases. Scanning electron microscopy (SEM) was used to assess the morphology of the surface of the steel samples after the samples had been immersed for 24 h in the extraction solution. The corrosion protection in the solutions with clay nanocarriers containing MBT and MBI was better than that in solutions without MMT. The UV-Vis results showed that the release of MBI species from Na^+-MMT nanocarriers in neutral pH was far lower than that of MBT species.

Keywords: azole derivatives; clay minerals; release; electrochemical impedance spectroscopy; corrosion inhibition

1. Introduction

Corrosion of metals is one of the most expensive problems in the field of materials science and engineering, with roots in the period of metal discovery [1]. Corrosion is defined as a gradual degradation in the properties of metals as a result of chemical or electrochemical reactions with their surrounding environment. Using corrosion inhibitors is one of the most effective protective measures against corrosion [1]. Azole organic materials such as 2-mercaptobenzothiazole (MBT) and 2-mercaptobenzimidazole (MBI) have a wide range of applications, including acting as corrosion inhibitors for the protection of various metal surfaces [2–3]. However, the structures of these organic materials contain many sulfur groups, which act as antifungal and antibacterial compounds [4–7]. If a corrosion inhibitor is used in a coating, its solubility becomes important; that is, the solubility of the inhibitor should be appropriate for the application [8]. If the solubility of the corrosion inhibitor is too low, its density will be limited in a corrosive environment, adversely affecting its inhibition ability. However, if its solubility is too high, the inhibitor may well protect the metal surface but quickly release into the corrosive environment, decreasing its density in the coating. Also, high solubility can result in osmotic pressure, eventually leading to blister formation and separation of the organic coating from the substrate [8]. Thus, the inhibitor should be encapsulated to enable its controlled release.

Thus far, many studies have been conducted on embedding azole organic inhibitors in carriers and using them in coatings. Various methods have been proposed for this purpose, including using porous-spherical-structured nanoparticles such as SiO_2 [9–10], halloysite nanotubes (HNTs) [11–14], and single-walled carbon nanotubes (SWCNTs) [15]; anionic clays such as layered double hydroxides (LDHs) [8,16]; polymeric microcapsules [17–18]; beta-cyclodextrin (β-CD) [19–20]; and gamma-cyclodextrin (γ-CD) [21]. Sodium montmorillonite (Na^+-MMT) is an important carrier that has not yet been sufficiently investigated.

MMT, a commercial layered silicate, has been widely

Corresponding author: Davood Zaarei E-mail: d_zarei@azad.ac.ir

used for preparing polymer nanocomposites. This mineral consists of silicate layers with a diameter of approximately 100 nm and a thickness of 1 nm and includes an ammonium hydroxide or magnesium hydroxide octagonal plate placed between two combined tetrahedral silicate layers. To achieve partial hydrophobicity, hydrophilic cations such as Na^+ ions should be replaced with organic cations such as alkyl ammonium in the space between the silicate layers, resulting in the formation of organophilic MMT. By reducing the surface energy of the silicate layers, the organic cations increase the mixing of layers with the polymer matrix and make it easier for the polymer to fit between the layers [22]. The arrangement of MMT in the coatings can increase their barrier property, thereby increasing their corrosion resistance by increasing the length of oxidizing agents' diffusion path into the coatings [23].

Ghazi *et al.* [24] inserted benzimidazole (BI) and Zn inhibitors into the interlayer space of Na^+-MMT. They then dispersed these hybrid materials as anticorrosion nanopigments in an epoxy ester polymeric matrix. Finally, they used electrochemical impedance spectroscopy (EIS) to investigate the anticorrosion behavior of the coatings after the specimens had been immersed for 25 d in 3.5wt% NaCl solution. Bode plots of the EIS data revealed that the epoxy ester coatings containing MMT + BI and MMT + Zn coatings exhibited higher corrosion resistance than epoxy coatings without the nanopigment. This anticorrosion behavior is attributable to multiple factors: the sheet-like structure of the MMT particles and the release of BI and Zn inhibitors from the interlayer space of the clay, each of which inhibits corrosion via a different mechanism of action. The BI inhibitors enhance the anticorrosion properties by blocking anodic and cathodic regions and forming a hydrophobic layer. By contrast, Zn, as a cathodic inhibitor, participates in the cathodic half-reaction and forms a protective layer of zinc hydroxide in cathodic regions.

Mehrabian and Sarabi Dariani [25] loaded 2-benzylbenzimidazole (2-BBI) as an inhibitor into a Na^+-MMT nanocarrier via an ion-exchange method, dispersed the loaded nanocarrier as an anticorrosion nanopigment in an epoxy polymeric matrix at concentrations of 1wt%, 2wt%, and 3wt%, and applied the polymer onto carbon steel. Finally, they used EIS to evaluate the corrosion resistance behavior of the resultant nanocomposite coatings after 120 d of immersion in 3.5wt% NaCl solution. The resulting Bode diagram showed that the epoxy coating containing 3wt% BBI-MMT nanopigment demonstrated the best corrosion resistance (~$1 \times 10^9\ \Omega$) after 120 d of immersion. The Bode figures also indicated that epoxy coatings containing 2wt% and 1wt% BBI-MMT nanopigment had impedance values of 10^8 and $10^7\ \Omega$, respectively. The impedance of an epoxy coating without the nanopigment was dramatically lower ($10^4\ \Omega$).The corrosion resistance of these coatings was attributed to a synergistic effect between the Na^+-MMT and the 2-BBI inhibitor.

Notably, most previous investigations in the field of azole-modified layered silicates have merely focused on polymeric nanocomposite coatings; their behavior in electrolyte media in the absence of polymeric matrices has not been studied. Therefore, in the present study, sulfur-containing azole derivatives (MBT and MBI) were introduced into the clay galleries of Na^+-MMT. The corrosion protection behavior of these hybrid compounds on mild steel in corrosive media was studied using electrochemical test methods.

2. Experimental

2.1. Materials

MBT, MBI, and ethyl alcohol were purchased from Merck Company (Germany). Na^+-MMT was provided by the US Rockwood Company.

2.2. Synthesis of the hybrid nanocompounds

To synthesize the compounds, 5 g of Na^+-MMT was dispersed in 350 mL of ethyl alcohol and stirred with a magnetic stirrer for 1 h [7]. This process resulted in swelling of the clay platelets [7]. In another vessel, 2 g of MBT and MBI was dissolved into 100 mL of ethyl alcohol by manual mixing, and the resultant mixture was transferred to the vessel containing Na^+-MMT. The resultant solution was stirred with a magnetic stirrer for 24 h at room temperature to insert the MBT and MBI molecules into the interlayer space of the clay particles. After this period of magnetic stirring, the solution was maintained at rest for 48 h to precipitate. On the basis of our previous work [7], a centrifuge (model EBA21, Hettich Company, Germany) was used to separate the synthesized modified clay compounds; the samples were centrifuged at 6000 r/min for 15 min. The sediments were washed with deionized water and kept in a vacuum oven for 24 h, thereby producing a dry and light powder.

2.3. Preparation of extract solution and surface of mild steel for electrochemical tests

To prepare the extract of the electrolyte solution under neutral (pH 7) conditions, a solution containing MMT + MBT, MMT + MBI, MBT, MBI, or Na^+-MMT, each as 1 g, was dispersed in 1 L of 3.5wt% NaCl solution for 48 h under magnetic stirring at 600 r/min. The blank electrolyte so-

lution for comparing the electrochemical results contained only 3.5wt% NaCl. The precipitated materials were subsequently collected using a centrifuge, followed by a filtration process. The extract solution containing the released material was analyzed.

For the electrochemical tests, 1 cm × 1 cm mild steel plates were prepared using 400- and 800-grit emery cloths and then degreased with methanol. The mild steel samples with different sizes were provided by Mobarakeh Steel Company (Iran). The elemental composition of the mild steel is listed in Table 1.

Table 1. Elemental composition of the mild steel samples wt%

C	Si	Mn	Cr	Mo	Co	Cu	Nb	Fe
0.190	0.288	1.390	0.026	0.018	0.388	0.297	0.334	97.06

As shown in Table 1, Fe accounts for the highest elemental content. The properties of the other components are summarized as follows:

Mn is found in many commercial steels, where its primary purpose is to increase the hardenability and strength of the steel. The carbon content directly affects the strength and hardenability of steel, specifically strength and hardenability increase through increasing carbon content [26]. Similar to Mn, Si is found in all steel grades; although its concentration is lower than that of Mn, it still increases the strength and hardness. It also plays an important role as a deoxidizer to inhibit defects and/or damage [26]. The key attribute of Cr is its ability to impart corrosion resistance to alloys in oxidizing media. The hardenability of steel is mostly enhanced by Cr which is considered the most powerful element regarding its influence on the physical and mechanical properties of steel [26]. Mo also strongly affects the properties of steel, its tensile strength, heat resistance and weldability [26].Co can augment the hardness and the yield point of steel; furthermore, it exhibits some antioxidant properties; in so being, it is used in heat-resistant steels and heat-resistant alloys. Nb can improve hardness, ductility, and wear and corrosion resistance [26]. The major function of Cu is to boost the atmospheric corrosion resistance of ordinary low-alloy steel, particularly in combination with P [26]. Thus, if the chemical composition of mild steel is known, its corrosion current density and potential can be predicted [27–29].

Notably, the literature contains limited information about the fundamental effects of grain size of mild steel and its relation to the corrosion resistance of this alloy in NaCl electrolyte solution. As indicated in Refs. [30–32], the corrosion resistance of mild carbon steel is lower for fine-grained steel specimens than for specimens with relatively coarser grains.

2.4. Characterization

The polarization tests were performed using a Corrtest CS350 (China) potentiostat/galvanostat and a common three-electrode system that included a saturated calomel reference electrode for controlling the applied potential in uncoated samples, a Pt auxiliary electrode for establishing the current, and a working electrode of an uncoated mild steel sample. These tests were carried out in the potential range of ±200 mV with a scan rate of 0.5 V/s. The corrosion current density and other information were obtained via the Tafel extrapolation method. Additionally, these tests were performed at room temperature and were repeated three times to enhance the accuracy of testing of similar samples.

EIS was performed using a Corrtest CS350 potentiostat/galvanostat in conjunction with a common three-electrode system that included a reference electrode, an auxiliary electrode, and a steel sample (1-cm^2 area) as the working electrode. Sample preparation for EIS was similar to that for the polarization tests. The EIS experiments were conducted at open-circuit potential (OCP) using ±10 mV perturbation in a frequency range from 10 kHz to 10 MHz after the samples had been immersed for 1, 4, 24, or 48 h. Frequency response analyzer software was used for data analysis.

The morphology of the surface of the steel samples after immersion in extracted solutions was analyzed by scanning electron microscopy (SEM) on a ZEISS Sigma VP-500 (Germany) scanning electron microscope. The samples were covered with a thin layer of gold via a physical vapor deposition (PVD) technique through the sputtering method.

According to the assigned objectives, X-ray diffraction (XRD) studies on the Na^+-MMT and the hybrid synthesized compounds were carried out on a Bruker SAXS D8 small-angle X-ray diffractometer (Cu K_α radiation, 40 kV, and 35 mA). The data were collected for angles (2θ) from 2° to 20°. The basal spacing d_{001} was calculated from the basal reflections using Bragg's law [7].

Ultraviolet-visible (UV-Vis) spectroscopy (Perkin-Elmer Lambda 25 spectrometer) was used to characterize the release behavior of MBT and MBI from the intercalated Na^+-MMT nanocarriers under neutral pH conditions. The release experiments were performed over the course of 48 h at room temperature. The preparation of extracts in a neutral environment is fully elaborated in section 2.3.

3. Results and discussion

3.1. Electrochemical impedance spectroscopy

The EIS results for samples immersed for 1, 4, 24, and 48 h in the electrolyte solution are shown in Figs. 1 and 2. Fig. 1

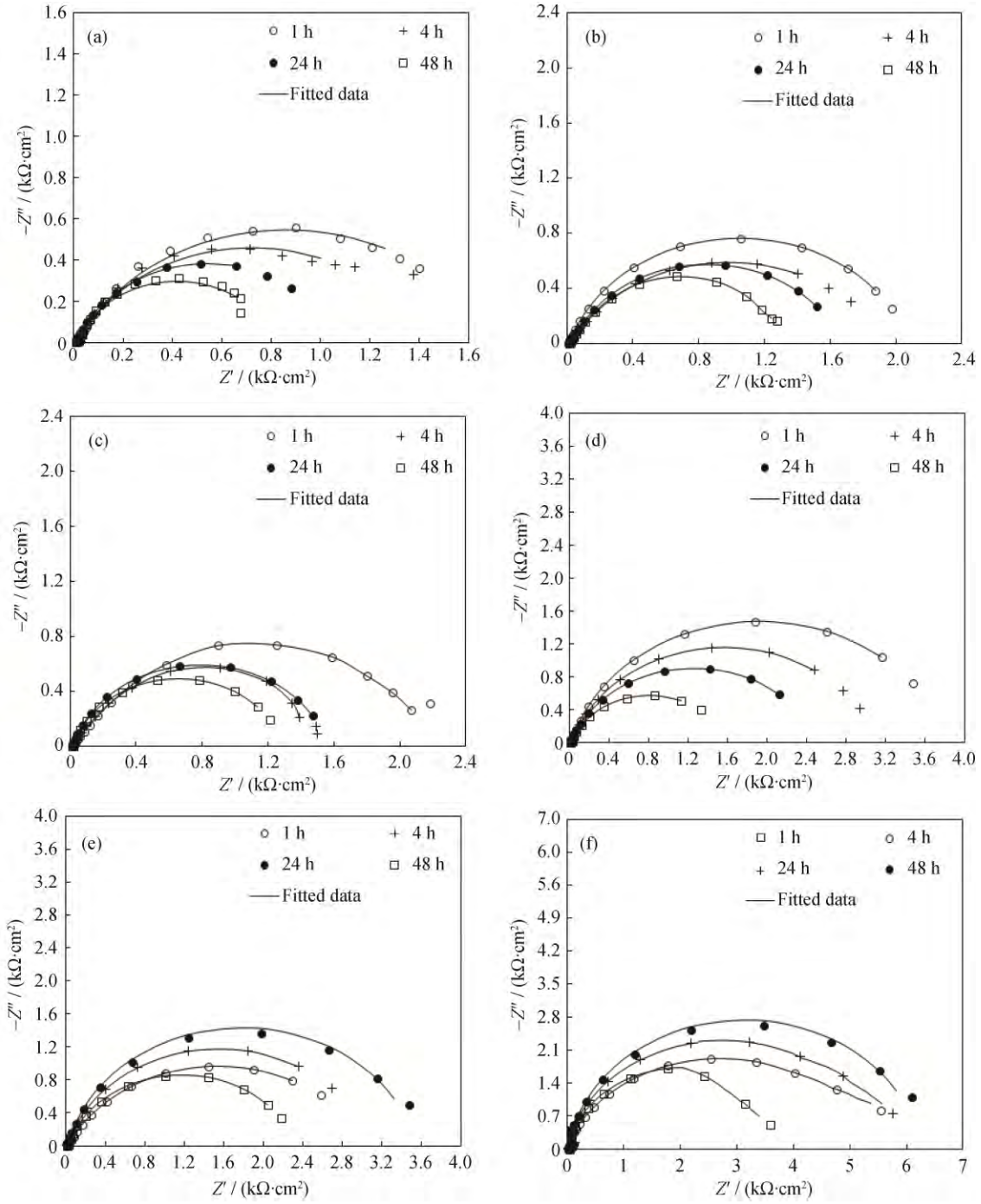

Fig. 1. Nyquist plots of the immersed mild steel samples after immersion for 1, 4, 24, and 48 h in different solutions: (a) blank; (b) Na^+-MMT; (c) MBI; (d) MBT; (e) MMT + MBI; (f) MMT + MBT.

shows that the diameter of the semicircle, which represents the charge transfer resistance in the double electric layer of the blank sample, is consistently smaller than those of the other samples, indicating its corrosion and destruction in the NaCl solution. The semicircle diameters corresponding to extracted solutions containing organic inhibitors or nanoclays (Figs. 1(b), 1(c), and 1(d)) are larger than that of the blank sample, which indicates an inhibition effect on the mild steel. However, the values of the real and imaginary resistance of these plots show that these materials are not suitable for the long-term protection of the metal surface and that corrosion will occur. For the extracted solutions containing the hybrid combinations (Figs. 1(e) and 1(f)), the diameters of the semicircles increased, indicating an improvement in the corrosion resistance of these systems. Unlike the extracted solutions containing MBT, MBI, and

Na^+-MMT, the semicircle diameters for MMT + MBI and MMT + MBT increased over time, indicating corrosion protection and a synergistic effect. Notably, for the sample of MMT + MBI, The semicircle diameter after 48 h is smaller than that after 24 h. It also decreases. But it is larger than that after 1 h, whereas that for the MMT + MBT sample increased, indicating better corrosion protection performance.

Fig. 2 shows the Bode plots used to evaluate the corrosion protection of the mild steel samples in different

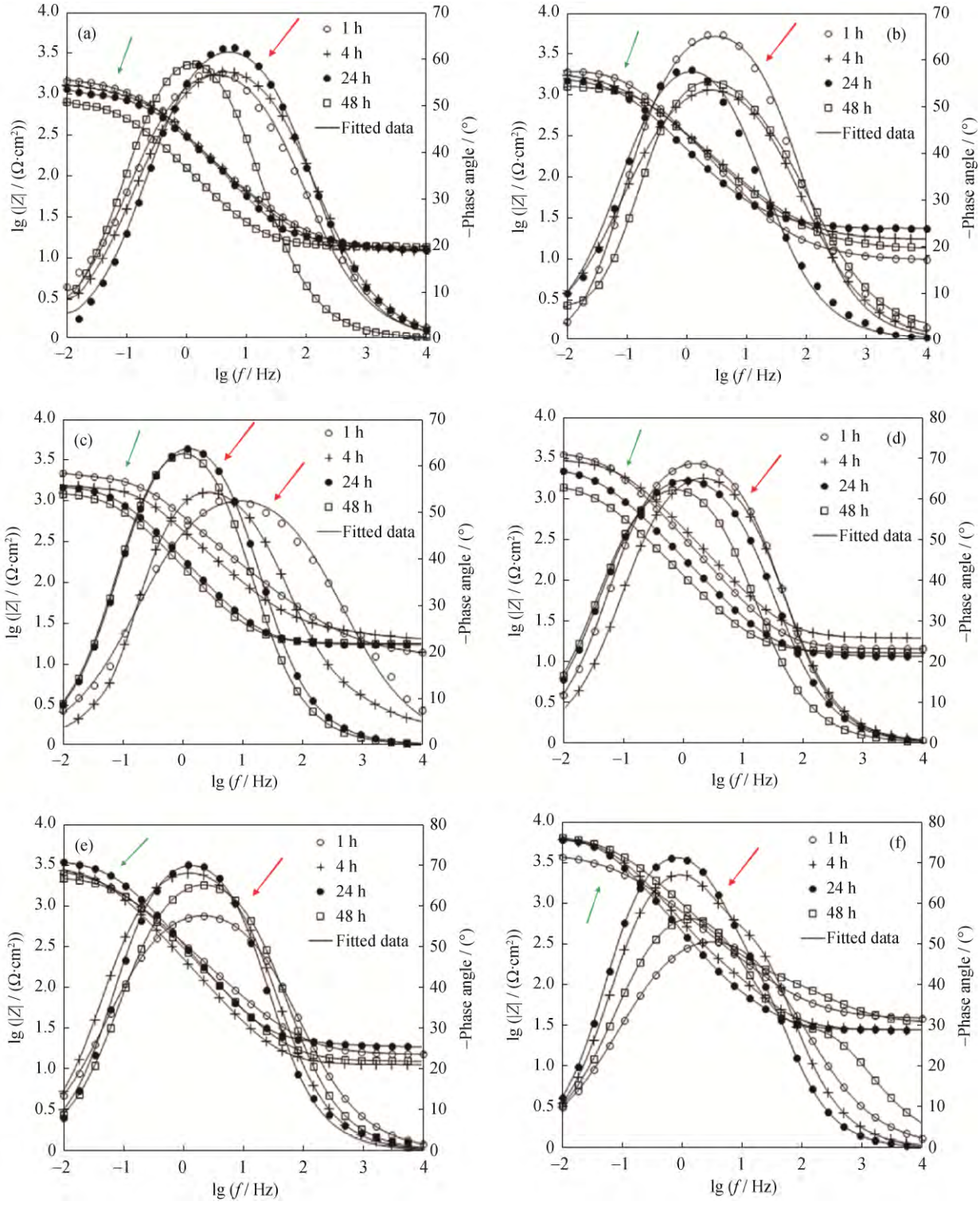

Fig. 2. Bode plots of the mild steel samples after immersion for 1, 4, 24, and 48 h in different solutions: (a) blank; (b) Na^+-MMT; (c) MBI: (d) MBT; (e) MMT + MBI; (f) MMT + MBT. Green and red arrows illustrate lg|*Z*| and phase angle lines, respectively.

solutions. In these figures, a single time constant is observed for the extracted solutions containing MBI, MBT, Na^+-MMT, or MMT + MBI, whereas a double time constant is observed after 4 h for the sample immersed in an extracted solution containing MMT + MBT, indicating the generation of an inhibitor sediment layer on the metal surface. The equivalent circuits used for fitting the data of the single and double time constant systems are shown in Fig. 3. The double time constant in the bode plot corresponding to steel corrosion protection in the MMT + MBT solution (Fig. 2(f)) might be due to the adsorption of the inhibitor onto steel surface. This adsorption process led to a small low-frequency loop observed as a resistance and confirmed by the data in Table 2. This resistance is parallel with a capacitance of the adsorbed film; the constant phase element (CPE) of the film is represented as CPE_f in Fig. 3.

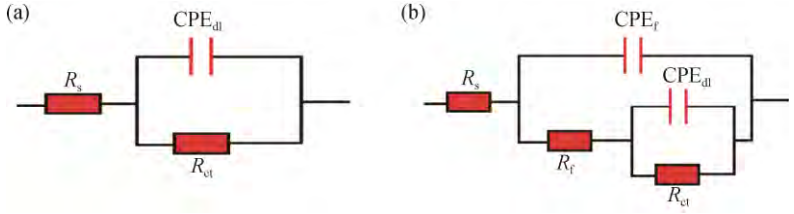

Fig. 3. Electrical equivalent circuits used for modeling the impedance curves with (a) single-time-constant and (b) double-time-constant circuits.

Table 2. Obtained electrochemical parameters from EIS tests on the mild steel specimens immersed in the extracted solutions for 1, 4, 24, and 48 h

Solution	Time / h	R_{ct} / ($\Omega\cdot cm^2$)	$Y_{0,dl}$ / ($\mu s^n\cdot\Omega^{-1}\cdot cm^{-2}$)	n_{dl}	C_{dl} / ($\mu F\cdot cm^{-2}$)	$R_f^{\dagger}$ / ($\Omega\cdot cm^2$)	$Y_{0,f}$ / ($\mu s^n\cdot\Omega^{-1}\cdot cm^{-2}$)	n_f	C_f / ($\mu F\cdot cm^{-2}$)	lg ($\lvert Z\rvert/(\Omega\cdot cm^2)$)	η_{imp} / %
Blank	1	1602	591.6	0.81	34	—	—	—	—	3.16	—
	4	1430	753.4	0.8	43.2	—	—	—	—	3.1	—
	24	1021.5	1034.6	0.79	56.9	—	—	—	—	3.06	—
	48	810.8	1218.2	0.8	68.3	—	—	—	—	2.9	—
MBI	1	2451	378.2	0.66	11.1	—	—	—	—	3.35	53
	4	1624	501.6	0.73	19.8	—	—	—	—	3.19	11.9
	24	1557	530	0.83	31.8	—	—	—	—	3.17	34.4
	48	1286	545	0.84	32.8	—	—	—	—	3.07	36.9
MBT	1	3829	604.9	0.84	45.8	—	—	—	—	3.55	58.1
	4	3112	481.2	0.82	31.7	—	—	—	—	3.47	54
	24	2506	1118.5	0.8	81.3	—	—	—	—	3.34	59.2
	48	1603	2004.5	0.79	148.2	—	—	—	—	3.14	49.4
Na^+-MMT	1	2081	641.7	0.81	40	—	—	—	—	3.26	23
	4	1939	776.2	0.7	34.5	—	—	—	—	3.24	26.2
	24	1635	706.4	0.77	37	—	—	—	—	3.18	37.5
	48	1436	715	0.72	29.5	—	—	—	—	3.11	43.5
MMT + MBI	1	3057	716.5	0.71	38.5	—	—	—	—	3.42	47.6
	4	3089	937.2	0.83	72.8	—	—	—	—	3.45	53.7
	24	3532	578.9	0.87	45.7	—	—	—	—	3.55	70.8
	48	2328	694.8	0.81	45.3	—	—	—	—	3.34	65.2
MMT + MBT	1	4216	342.5	0.66	12.6	—	—	—	—	3.57	62
	4	6080	82.9	0.95	7.1	502.1	264.9	0.83	10.9	3.79	76.5
	24	6358	28.3	0.9	1.8	154.6	280.4	0.89	14.3	3.79	83.9
	48	6947	23.5	0.79	0.8	142.4	99.5	0.7	0.6	3.82	88.3

Note: $Y_{0,dl}$ is the admittance of the constant phase element of double layer, $Y_{0,f}$ is the admittance of the constant phase element of inhibitor film, n_{dl} is the exponent of the constant phase element of double layer, n_f is the exponent of the constant phase element of inhibitor film, and $R_f^{\dagger}$ is the resistance of inhibitor film.

In the circuits in Fig. 3, R_s is the solution resistance, R_{ct} is the charge transfer resistance, CPE_{dl} is the constant phase element denoting the electric double layer, and R_f and CPE_f respectively represent the resistance and the constant phase element of the inhibitor film. The capacitance of the double layer (C_{dl}) were obtained through Eq. (1):

$$C_{dl} = (Y_0 \cdot R^{1-n})^{1/n} \quad (1)$$

where Y_0 is the admittance of the CPE and n is a constant related to surface heterogeneity. The values of the electrochemical parameters resulting from three fittings for the data corresponding to 1, 4, 24, and 48 h of immersion were calculated; the average of the results is presented in Table 2. According to the results in Table 2, the charge transfer resistance values for the solutions containing the organic inhibitors, Na^+-MMT, and the hybrid materials increased compared with the charge transfer resistance value for the blank sample. These results indicate improved corrosion resistance in the presence of the aforementioned compounds. Table 2 shows that, with increasing immersion time, the R_{ct} values of the extracted solutions containing MBI, MBT, Na^+-MMT, MMT + MBI and blank decreased, whereas those of the solutions containing MMT + MBT increased. The larger R_{ct} values indicate an enhanced ability of current to pass through the capacitor in the circuit.

As shown in Table 2, after specimens were immersed in the electrolyte for 48 h, the charge transfer resistance and impedance inhibition efficiency (η_{imp}) of the extracted solution of MMT + MBT is greater than that of the extracted solutions of the other compounds. This result indicates better corrosion inhibitory properties of the MMT + MBT, which might also be related to the synergistic effects of the organic inhibitor and the mineral clay as well, through adsorption onto the steel surface and formation of a protective layer. In the case of charge transfer resistance, the steel samples immersed in the solution containing MMT + MBT exhibited larger values than the steel samples immersed in the solution containing MMT + MBI. The charge transfer resistance of the specimen immersed in MMT + MBT for 48 h was equal to 6947 $\Omega \cdot cm^2$, which is higher than that of the specimen immersed in MMT + MBI (2328 $\Omega \cdot cm^2$). For a 24 h immersion time, MMT + MBI accounted for the highest charge transfer resistance, thereby followed by a descending trend, while the samples containing MMT + MBT had an increased charge transfer resistance in the immersion time range of 1 to 48 h. For MMT + MBT, a second time constant appeared in the high-frequency region after only 4 h of immersion, which indicates the generation of a compact inhibition layer for this sample. The second time constant for the solution containing MMT + MBI was not clear, indicating that the noted times were insufficient for generating the inhibition layer and that, even if this deposited layer was generated, the time constant would be similar to the corrosion-related time constant.

Table 2 also shows that the lowest admittance value among the samples was observed for the solution containing MMT + MBT and that a similar performance was observed for the electric double layer capacitance. Decreases in the admittance values and the capacitance of the double layer can generate an inhibition layer or increase the thickness of the electric double layer. These results clearly demonstrate the inhibition and synergistic performance of MMT + MBT. The impedance values at 10 MHz, as obtained from Fig. 2, are reported in Table 2. These values are similar to those of the charge transfer resistance. The impedance values for the steel samples immersed in the solution containing MMT + MBT are higher than those for the other samples. This sample exhibited a higher impedance value at all immersion times, indicating its better corrosion-inhibition performance compared with those of the other samples. The impedance inhibition efficiency was calculated by Eq. (2):

$$\eta_{imp} = \left(1 - \frac{R_{ct,blank}}{R_{ct}}\right) \times 100\% \quad (2)$$

The inhibition efficiency results are in accordance with the other results.

The EIS results clearly show that the interaction of the clay nanoparticles with the organic inhibitors efficiently improves the corrosion-inhibition performance of the system. The enhanced inhibition performance of MMT + MBT compared with that of MMT + MBI might be related to the greater inhibition effect of MBT compared with that of MBI. This enhanced inhibition effect of MBT is attributable to the greater surface coverage area of MBT and its greater adsorption power compared with that of MBI [17,33]. The amount of material adsorbed and the formation of a passive layer govern the protection performance against corrosive species.

3.2. Polarization tests

The polarization curves for samples immersed for 24 h in the extracted solutions are presented in Fig. 4.

The polarization curves show that the corrosion current density for the blank sample was equal to 18.5 $\mu A/cm^2$. After the aforementioned compounds were added into the sodium chloride (3.5wt%) electrolyte solution, the corrosion current density of the samples decreased substantially compared with that of the blank sample. In the case of Na^+-MMT, the corrosion current density decreased to 14.4 $\mu A/cm^2$, representing a modest change. For the extracted solutions containing the hybrid combinations of MMT + MBT and MMT + MBI, the decreases were more dramatic, resulting in corrosion current densities of 3.3 and 4.6 $\mu A/cm^2$,

respectively. Also, the corrosion potential of the MBI sample was approximately −698 mV, whereas that of the blank sample was −685 mV; however, the corrosion potential of the Na^+-MMT sample shifted to the more negative value of −701 mV, which is related to the cathodic inhibition mechanism.

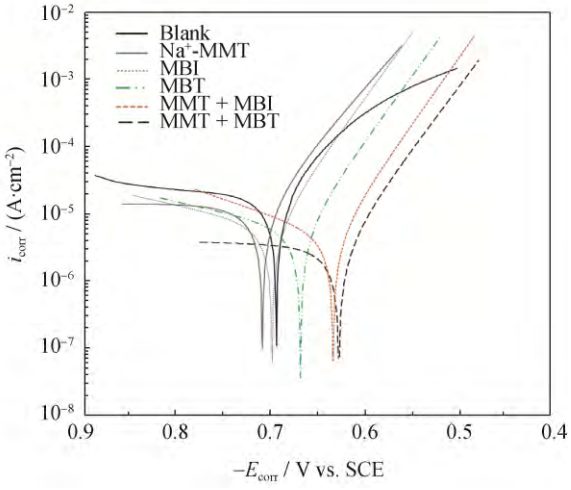

Fig. 4. Polarization curves for the samples immersed in the extracted solutions of 3.5wt% NaCl (blank), Na^+-MMT, MBI, MBT, MMT + MBI, and MMT + MBT for 24 h.

Fig. 4 shows that the specimens immersed in extracted solutions containing MBT, MMT + MBT, and MMT + MBI shifted to more positive values of −668, −626, and −633 mV, respectively, which is likely related to the anodic inhibition mechanism; however, for the hybrid combinations, both the anodic and the cathodic branches shifted toward lower currents, indicating mixed corrosion inhibition [34]. These hybrid materials often have a dominant anodic and cathodic effect. A decrease in the corrosion current density and an increase in the potential are consequence of the inhibitor sediment layer on the steel surface, which blocks the active anodic and cathodic areas and limits attacks by corrosive species on the surface [35–37]. The positive potential of MMT + MBT and MMT + MBI confirms the good corrosion-inhibition performance of these hybrid combinations in the electrolyte because the presence of Na^+-MMT can affect the reduction reaction of H_2 and O_2 and react with the OH^- ions in the cathode area, which results in insoluble compounds and prevents oxygen from reaching the cathode area [8,24]. However, the presence of the corrosion inhibitors MBT and MBI in hybrid combinations enhances their physical and chemical absorption onto the metal surface [13,34]. Physisorption can occur through proton-accepting or proton-donating behavior of the aforementioned inhibitors in different environments, and chemisorption can occur through chemical bonding via electron transfer from the lone pair of N with the vacant *d* orbital of the metal atom [13,34]. Also, these inhibitors are gathered on the metal surface, where they create a protective hydrophobic layer composed of adsorbed molecules, which functions as a barrier to metal dissolution into the electrolyte [13,34].

Finally, the combinations of MMT + MBT and MMT + MBI showed a polarization inhibition efficiency (η_p) of 82% and 75%, respectively, representing the highest and second-highest values, respectively, among the investigated inhibitors. Electrochemical corrosion parameters such as the corrosion potential (E_{corr}), corrosion current density (i_{corr}), anodic Tafel slope (b_a), and cathodic Tafel slope (b_c) were obtained through Tafel extrapolation after the specimens were immersed for 24 h; the results are reported in Table 3.

The polarization inhibition efficiency was obtained through the following equation:

$$\eta_p = \frac{i_{corr,blank} - i_{corr}}{i_{corr,blank}} \times 100\% \quad (3)$$

where $i_{corr,blank}$ is the corrosion current density of electrolyte solution containing no inhibitor.

Table 3. Electrochemical parameters obtained from polarization with Tafel extrapolation for specimens of mild steel immersed in the extracted solutions for 24 h

Solution	E_{corr} / mV vs. SCE	i_{corr} / (μA·cm^{-2})	b_a / (V·decade^{-1})	$-b_c$ / (V·decade^{-1})	η_p / %
Blank	−685	18.5	0.11	0.41	–
MBI	−698	6.6	0.05	0.3	64
MBT	−668	5.7	0.2	0.31	69
Na^+-MMT	−701	14.4	0.09	0.6	22
MMT + MBI	−633	4.6	0.21	0.5	75
MMT + MBT	−626	3.3	0.4	0.58	82

3.3. Release study of the inhibitors

Fig. 5 shows the amount of MBI and MBT inhibitors released from the Na^+-MMT nanocarriers in neutral environments. Calculations for release percentage were obtained from reference [38].

After 48 h, the release amount of MBT inhibitor from the Na^+-MMT nanocarrier in a neutral environment was approximately 42%, whereas MBI inhibitor exhibited a lower release

amount 27% during the same time period. The controlled release of inhibitors into corrosive environments over long periods of time leads to good protection of metal surfaces.

3.4. SEM results

The surface of the steel samples after 24 h of immersion in extracted solutions was analyzed by SEM; the results are illustrated in Fig. 6. As shown in Fig. 6(a_1), the surface of the metal was smooth before immersion in the electrolyte solution. After immersion in electrolyte Fig. 6(a_2), the surface of the mild steel was corroded.

The micrographs of the samples immersed in the extracted solutions containing organic inhibitors (MBI and

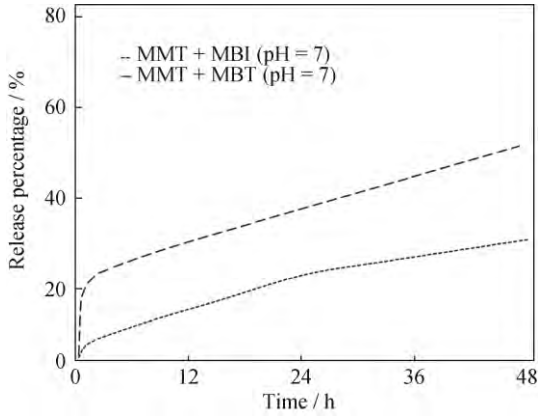

Fig. 5. Release rate of corrosion inhibitors from Na^+-MMT nanocarriers containing MBI and MBT.

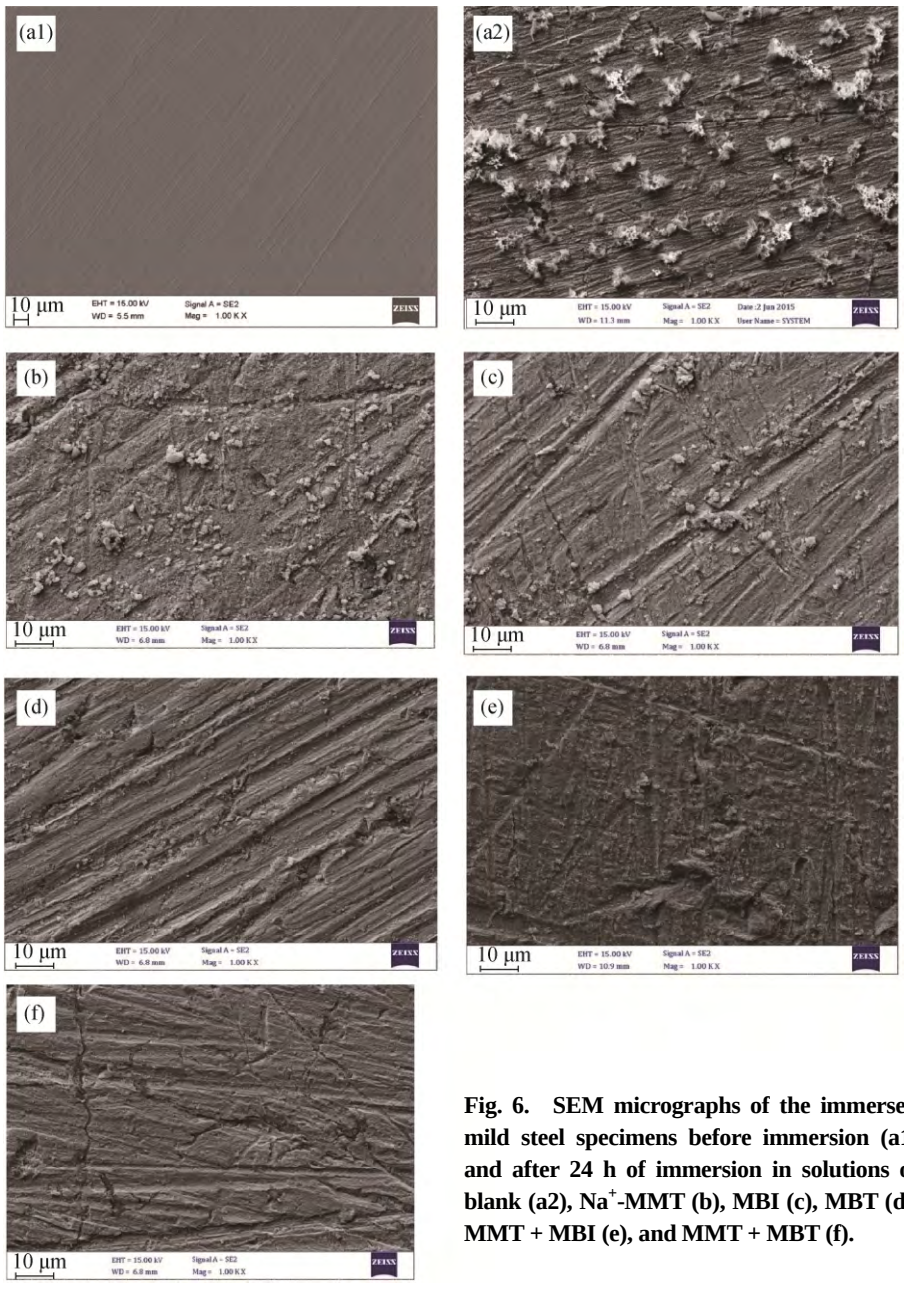

Fig. 6. SEM micrographs of the immersed mild steel specimens before immersion (a1) and after 24 h of immersion in solutions of blank (a2), Na^+-MMT (b), MBI (c), MBT (d), MMT + MBI (e), and MMT + MBT (f).

MBT), Na^+-MMT, and the hybrid combinations MMT + MBI and MMT + MBT show the construction of adsorbed film containing sediments (Figs. 6(b)–6(f)). Corrosion products are evident in (Figs. 6(a_2), 6(b), and 6(c)). The surfaces of steel immersed in solutions containing MBT, MMT + MBI, and MMT + MBT (Figs. 6(d), 6(e), and 6(f)) are free of corrosion products, indicating better protection of these materials through the presence of suitable corrosion protection species. Fig. 6(f), immersion into the solution containing MMT + MBT, shows that the constructed film is more uniform and steady, which is the best diagnosed reason for the inhibitive film effects observed in the EIS tests. That is a suitable relationship exists between the constructed protective film on the surface and the inhibition–corrosion performance: the more the film layer thickness on the surface, the better the corrosion-inhibition performance.

3.5. XRD analysis of hybrid nanocompounds

Fig. 7 shows the small-angle XRD patterns of Na^+-MMT, MMT + MBT, and MMT + MBI. The maximum peak for Na^+-MMT at $2\theta = 7.4°$ indicates that the distance between the clay plates is approximately 1.14 nm [7]. The XRD patterns for the hybrid nanocompounds MMT + MBT and MMT + MBI show peaks at $2\theta = 4.9°$ and $2\theta = 4.5°$; therefore, the distances between the clay plates increased to 1.80 and 1.93 nm, respectively. These results indicate that the molecules of the organic materials (MBT and MBI) penetrated the interlayer space (gallery). The diffraction characteristics of the Na^+-MMT and the hybrid synthesized nanocompounds are summarized in Table 4.

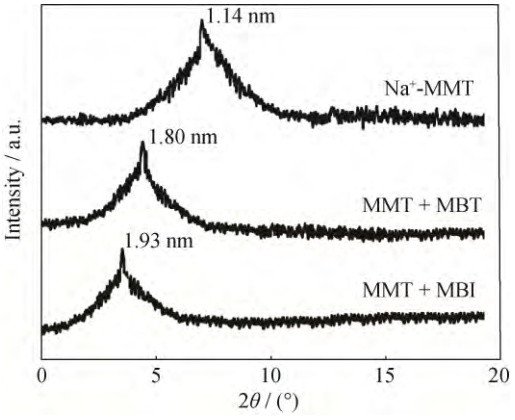

Fig. 7. XRD patterns of Na^+-MMT, MMT + MBI, and MMT + MBT.

Table 4. Interlayer distances of Na^+- MMT, MMT + MBI, and MMT + MBT systems, as determined by XRD

Sample	2θ / (°)	d_{001} / nm	Δd / nm
Na^+-MMT	7.4	1.14	—
MMT + MBT	4.9	1.80	0.66
MMT + MBI	4.5	1.93	0.79

4. Conclusions

MBT and MBI were introduced as corrosion-inhibiting species into the interlayer of montmorillonite clay; the resultant compounds were characterized, and their corrosion-inhibiting properties in NaCl solution were studied. The results are summarized as follows.

(1) XRD analysis showed that MBT and MBI were intercalated into clay layers and that the *d*-spacings of these materials increased by 0.66 nm and 0.79 nm, respectively.

(2) The corrosion protection of mild steel in NaCl solutions containing azole-modified layered silicates (MMT + MBT and MMT + MBI) was far greater than that of solutions containing only MBT, MBI, or Na^+-MMT. The corrosion protection efficiencies of MMT + MBT and MMT + MBI were approximately 88.3% and 65.2%, respectively.

(3) The UV-Vis results indicated that the release of MBT and MBI species from Na^+-MMT nanocarriers in neutral pH were 42% and 27%, respectively.

(4) SEM observations indicated that a compact deposited layer was created by the adsorbed molecules of MMT + MBT and MMT + MBI samples on the surface of mild steel. However, the MMT + MBT adsorbed surface was more uniform than those of the other samples.

References

[1] P.B. Raja, M. Ismail, S. Ghoreishiamiri, J. Mirza, M.C. Ismail, S. Kakooei, and A.A. Rahim, Reviews on corrosion inhibitors: A short view, *Chem. Eng. Commun.*, 203(2016), No. 9, p. 1145.

[2] A.C. Balaskas, M. Curioni, and G.E. Thompson, Effectiveness of 2-mercaptobenzothiazole, 8-hydroxyquinoline and benzotriazole as corrosion inhibitors on AA 2024-T3 assessed by electrochemical methods, *Surf. Interface Anal.*, 47(2015), No. 11, p. 1029.

[3] J.A. Calderón, F.A. Vásquez, and J.A. Carreño, Adsorption and performance of the 2-mercaptobenzimidazole as a carbon steel corrosion inhibitor in EDTA solutions, *Mater. Chem. Phys.*, 185(2017), p. 218.

[4] M.A. Azam and B. Suresh, Biological activities of 2-mercaptobenzothiazole derivatives: A review, *Sci. Pharm.*, 80(2012), No. 4, p. 789.

[5] M.F. Mahdi, R.F. Al-Smaism, and N.W. Ibrahim, Synthesis, characterization and antibacterial evaluation of novel 2-mercaptobenzothiazole derivatives bearing 2-aminonicotinonitrile moiety, *Eur. J. Chem.*, 7(2016), No. 1, p. 8.

[6] A. Kuznetsova, P.M. Domingues, T. Silva, A. Almeida, M.L. Zheludkevich, J. Tedim, M.G.S. Ferreira, and A. Cunha, Antimicrobial activity of 2-mercaptobenzothiazole released from

environmentally friendly nanostructured layered double hydroxides, *J. Appl. Microbiol.*, 122(2017), No. 5, p. 1207.

[7] M. Edraki and D. Zaarei, Modification of montmorillonite clay with 2-mercaptobenzimidazole and investigation of their antimicrobial properties, *Asian J. Green Chem.*, 2(2018), No. 3, p. 171.

[8] J. Tedim, S.K. Poznyak, A. Kuznetsova, D. Raps, T. Hack, M.L. Zheludkevich, and M.G.S. Ferreira, Enhancement of active corrosion protection via combination of inhibitor-loaded nanocontainers, *ACS Appl. Mater. Interfaces*, 2(2010), No. 5, p. 1528.

[9] K. Kermannezhad, A.N. Chermahini, M.M. Momeni, and B. Rezaei, Application of amine-functionalized MCM-41 as pH-sensitive nano container for controlled release of 2-mercaptobenzoxazole corrosion inhibitor, *Chem. Eng. J.*, 306(2016), p. 849.

[10] Y.C. Feng and Y.F. Cheng, An intelligent coating doped with inhibitor-encapsulated nanocontainers for corrosion protection of pipeline steel, *Chem. Eng. J.*, 315(2017), p. 537.

[11] K.A. Zahidah, S. Kakooei, M. Kermanioryani, H. Mohebbi, M.C. Ismail, and P.B. Raja, Benzimidazole-loaded halloysite nanotube as a smart coating application, *Int. J. Eng. Technol.*, 7(2017), No. 4, p. 243.

[12] D. Yu, J. Wang, W. Hu, and R. Guo, Preparation and controlled release behavior of halloysite/2-mercaptobenzothiazole nanocomposite with calcined halloysite as nanocontainer, *Mater. Des.*, 129(2017), p. 103.

[13] A. Joshi, E. Abdullayev, A. Vasiliev, O. Volkova, and Y. Lvov, Interfacial modification of clay nanotubes for the sustained release of corrosion inhibitors, *Langmuir*, 29(2012), No. 24, p. 7439.

[14] B.C. Zhong, Z.X. Jia, Y.F. Luo, B.C. Guo, and D.M. Jia, Preparation of halloysite nanotubes supported 2-mercaptobenzimidazole and its application in natural rubber, *Composites Part A*, 73(2015), p. 63.

[15] K.V. Yeole, I.P. Agarwal, and S.T. Mhaske, The effect of carbon nanotubes loaded with 2-mercaptobenzothiazole in epoxy-based coatings, *J. Coat. Technol. Res.*, 13(2016), No. 1, p. 31.

[16] Y.H. Dong, F. Wang, and Q. Zhou, Protective behaviors of 2-mercaptobenzothiazole intercalated Zn–Al-layered double hydroxide coating, *J. Coat. Technol. Res.*, 11(2014), No. 5, p. 793.

[17] R.J. Marathe, A.B. Chaudhari, R.K. Hedaoo, D. Sohn, V.R. Chaudhari, and V.V. Gite, Urea formaldehyde (UF) microcapsules loaded with corrosion inhibitor for enhancing the anti-corrosive property of acrylic-based multifunctional PU coatings, *RSC Adv.*, 5(2015), No. 20, p. 15539.

[18] F. Maia, K.A. Yasakau, J. Carneiro, S. Kallip, J. Tedim, T. Henriques, A. Cabral, J. Venâncio, M.L. Zheludkevich, and M.G.S. Ferreira, Corrosion protection of AA2024 by sol–gel coatings modified with MBT-loaded polyurea microcapsules, *Chem. Eng. J.*, 283(2016), p. 1108.

[19] A. Rahimi and S. Amiri, Anticorrosion hybrid nanocomposite coatings with encapsulated organic corrosion inhibitors, *J. Coat. Technol. Res.*, 12(2015), No. 3, p. 587.

[20] A. Altin, M. Rohwerder, and A. Erbe, Cyclodextrins as carriers for organic corrosion inhibitors in organic coatings, *J. Electrochem. Soc.*, 164(2017), No. 4, p. 128.

[21] A. Rahimi and S. Amiri, Self-healing anticorrosion coating containing 2-mercaptobenzothiazole and 2-mercaptobenzimidazole nanocapsules, *J. Polym. Res.*, 23(2016), No. 4, p. 83.

[22] M. Edraki and M.Banimahd Keivani, Study on the optical and rheological properties of polymer-layered silicate nanocomposites, *J. Phys. Theor. Chem. IAU Iran*, 10(2013), No. 1, p. 69.

[23] A.H. Navarchian, M. Joulazadeh, and F. Karimi, Investigation of corrosion protection performance of epoxy coatings modified by polyaniline/clay nanocomposites on steel surfaces, *Prog. Org. Coat.*, 77(2014), No. 2, p. 347.

[24] A. Ghazi, E. Ghasemi, M. Mahdavian, B. Ramezanzadeh, and M. Rostami, The application of benzimidazole and zinc cations intercalated sodium montmorillonite as smart ion exchange inhibiting pigments in the epoxy ester coating, *Corros. Sci.*, 94(2015), p. 207.

[25] N. Mehrabian and A.A. Sarabi Dariani, Anticorrosive performance of epoxy/modified clay nanocomposites, *Polym. Compos.*, 39(2018), E2134. DOI:10.1002/pc.24492.

[26] P. Pokorny, J. Kolisko, L. Balik, and P. Novak, Effect of chemical composition of steel on the structure of hot-dip galvanized coating, *Metalurgija*, 55(2016), No. 1, p. 115.

[27] N. Narimani, B. Zarei, H. Pouraliakbar, and G. Khalaj, Predictions of corrosion current density and potential by using chemical composition and corrosion cell characteristics in microalloyed pipeline steels, *Measurement*, 62(2015), p. 97.

[28] G. Khalaj, H. Pouraliakbar, N. Arab, and M. Nazerfakhari, Correlation of passivation current density and potential by using chemical composition and corrosion cell characteristics in HSLA steels, *Measurement*, 75(2015), p. 5.

[29] H. Pouraliakbar, G. Khalaj, M.R. Jandaghi, and M.J. Khalaj, Study on the correlation of toughness with chemical composition and tensile test results in microalloyed API pipeline steels, *J. Min. Metall. Sect. B*, 51(2015), No. 2, p. 173.

[30] K.D. Ralston and N. Birbilis, Effect of grain size on corrosion: A review, *Corrosion*, 66(2010), No. 7, p. 075005.

[31] H.W. Wang and C. Yu, Effect of grain size on corrosion properties of low alloy steel under H_2S/CO_2 environment, *Int. J. Electrochem. Sci.*, 12(2017), No. 5, p. 4327.

[32] P.K. Rai, S. Shekhar, and K. Mondal, Development of gradient microstructure in mild steel and grain size dependence of its electrochemical response, *Corros. Sci.*, 138(2018), p. 85.

[33] V.M. Abbasov, S.A. Mamedxanova, H.M.A. El-Lateef, L.I. Aliyeva, T.A. Ismayilov, M.C. Ilham, L.M. Afandiyeva, O.A.

Aydamirov, and F.A. Amirov, The CO_2 corrosion inhibition of carbon steel C1018 by some novel complex surfactants based on petroleum acids and nitrogen-containing compounds, *Adv. Mater. Corros.*, 2(2013), No. 1, p. 26.

[34] E. Abdullayev, V. Abbasov, A. Tursunbayeva, V. Portnov, H. Ibrahimov, G. Mukhtarova, and Y. Lvov, Self-healing coatings based on halloysite clay polymer composites for protection of copper alloys, *ACS Appl. Mater. Interfaces*, 5(2013), No. 10, p. 4464.

[35] N. Goudarzi and H. Farahani, Investigation on 2-mercaptobenzothiazole behavior as corrosion inhibitor for 316-stainless steel in acidic media, *Anti-Corros. Meth. Mater.*, 61(2013), No. 1, p. 20.

[36] G. Žerjav, A. Lanzutti, F. Andreatta, L. Fedrizzi, and I. Milošev, Characterization of self-assembled layers made with stearic acid, benzotriazole, or 2-mercaptobenzimidazole on surface of copper for corrosion protection in simulated urban rain, *Mater. Corros.*, 68(2017), No. 1, p. 30.

[37] K. Xhanari and M. Finšgar, The first electrochemical and surface analysis of 2-aminobenzimidazole as a corrosion inhibitor for copper in chloride solution, *New J. Chem.*, 41(2017), No. 15, p. 7151.

[38] A.R. Chandrasekaran, C.Y. Jia, C.S. Theng, T. Muniandy, S. Muralidharan, and S.A. Dhanaraj, Invitro studies and evaluation of metformin marketed tablets-Malaysia, *J. Appl. Pharm. Sci.*, 1(2011), No. 5, p. 214.